Ingeniare. Revista Chilena de Ingeniería
ISSN: 0718-3291
ingeniare@uta.cl
Universidad de Tarapacá
Chile

Ferrer Pacheco, Martha Yasmid; Vargas Galvis, Fabio; Vera López, Enrique; Moreno Téllez, Carlos Mauricio; Peña Rodríguez, Gabriel

Evaluation of morphology, wear and corrosion resistance of ZrO2-Al2O3/Ni coatings deposited on carbon steel substrates with flame spraying

Ingeniare. Revista Chilena de Ingeniería, vol. 25, núm. 4, diciembre, 2017, pp. 721-732
Universidad de Tarapacá
Arica, Chile

Evaluation of morphology, wear and corrosion resistance of ZrO_2-Al_2O_3/Ni coatings deposited on carbon steel substrates with flame spraying

Evaluación de la morfología, resistencia al desgaste y a la corrosión de recubrimientos de ZrO_2-Al_2O_3/Ni depositados sobre sustratos de acero al carbono mediante proyección térmica por llama

Martha Yasmid Ferrer Pacheco[1]* Fabio Vargas Galvis[2] Enrique Vera López[3]
Carlos Mauricio Moreno Téllez[3] Gabriel Peña Rodríguez[1]

Received: May 11, 2015 Accepted: October 3, 2016
Recibido 11 de mayo de 2015, aceptado 3 de octubre de 2016

ABSTRACT

The morphology, wear and corrosion resistance of bilayer coatings elaborated by flame spraying on AISI SAE 1020 substrates are reported. The first layer (bond coat) is a nickel-base alloy (CPM 1205^{TM}), and the second is a compound of ZrO_2-36 wt.% of Al_2O_3 (MetaCeram 25088^{TM}). The ceramic coating was deposited using oxidizing and super oxidizing flames, obtained from the fuel/comburent ratio of 1: 2.8 and 1: 4.3 respectively, at projection distances of 8, 9 and 10cm. The corrosion resistance was evaluated by electrochemical impedance spectroscopy (EIS),wear resistance was analyzed using a tribometer MicroTest in the ball-disc configuration, and the morphology was studied using scanning electron microscopy (SEM). The results showed a varied surface morphology of these coatings and the presence of bimodal areas formed by nanometric unmelted particles surrounded by melted particles. The wear resistance and Vickers microhardness of the ceramic coatings did not vary significantly with changes to the type of flame used and spray distance. By comparing the corrosion resistance of the substrate (AISI SAE 1020) and the coated samples, a significant increase of approximately 27 times was observed for these; moreover, it was reported that for coatings obtained using a super oxidizing flame, resistance to polarization increased with increasing spray distance, and for the oxidizing flame, the opposite behavior was observed. Overall, the results show the versatility of the thermal spray flame technique in forming bilayer coatings of ZrO_2-Al_2O_3/Ni that efficiently protect the surfaces of steel AISI SAE 1020 when exposed to corrosive and erosive environments.

Keywords: Flame spraying, wear, coatings, corrosion, ZrO_2-Al_2O_3/Ni, steel AISI SAE 1020.

RESUMEN

En este trabajo se reporta el comportamiento a la corrosión, al desgaste y morfología de recubrimientos bicapa elaborados por proyección térmica oxiacetilénica sobre sustratos de acero AISI SAE 1020.

[1] Universidad Francisco de Paula Santander. Facultad de Ciencias. Grupo de Investigación en Tecnología Cerámica (GITEC). Código postal: 540003. San José de Cúcuta, Colombia. E-mail: marthayasmidfp@ufps.edu.co, maryaferr@gmail.com; gpenaro@ufps.edu.co
[2] Universidad de Antioquia. Facultad de Ingeniería. Grupo de Investigación en Materiales Cerámicos y Recubrimientos (GIMACYR). Grupo de Investigaciones Pirometalúrgicas y de Materiales (GIPIMME).Código Postal: 050010. Medellín. Colombia. E-mail: fabio.vargas@udea.edu.co
[3] Universidad Pedagógica y Tecnológica de Colombia. Facultad de Ingeniería. Grupo de Integridad y Evaluación de Materiales (GIEM). Instituto para la Investigación e Innovación en Ciencia y Tecnología de Materiales (INCITEMA). Código postal: 150003. Tunja. Colombia. E-mail: enrique.vera@uptc.edu.co; carlosmauricio.moreno@uptc.edu.co
* Corresponding author.

La primera capa (bond coat) de una aleación base Ni (CPM 1205™) y la segunda de un compuesto de ZrO_2-36% en peso de Al_2O_3 (MetaCeram 25088™). El recubrimiento cerámico se depositó usando llama oxidante y súper-oxidante, obtenidas de la relación combustible/comburente 1:2,8 y 1:4,3, respectivamente, para distancias de proyección de 8, 9 y 10 cm. La resistencia a la corrosión fue evaluada por espectroscopia de impedancia electroquímica EIS, el desgaste fue analizado usando tribómetro MicroTest en configuración bola-disco, y la morfología se estudió usando microscopia electrónica de barrido (MEB). Los resultados evidencian una morfología superficial propia de este tipo de recubrimientos, así como la presencia de zonas bimodales formada de partículas nanométricas sin fundir rodeadas por partículas fundidas. Se encontró que la resistencia al desgaste y microdureza Vickers de los recubrimientos cerámicos no variaron significativamente al cambiar el tipo de llama y la distancia de proyección. Al comparar la resistencia a la corrosión de sustrato (acero AISI SAE 1020) y de las muestras recubiertas se observó para estas un incremento significativo de aproximadamente 27 veces, por otra parte, se reporta que para la llama súper-oxidante la resistencia a la polarización se incrementa al aumentar la distancia de proyección, mientras para la llama oxidante el comportamiento fue inverso. En general, los resultados muestran la versatilidad de la técnica de proyección térmica por llama, permitiendo realizar recubrimientos bicapas de ZrO_2-Al_2O_3/Ni eficientes para proteger superficies de acero AISI SAE 1020 expuestos a ambientes corrosivos y erosivos.

Palabras clave: Proyección térmica por llama, desgaste, recubrimientos, corrosión, ZrO_2-Al_2O_3 / Ni, acero AISI SAE 1020.

INTRODUCTION

The materials in turbines, exhaust pipes, fireplaces, furnaces, dryers, boilers and pipes, among others, are frequently exposed to both erosive and corrosive environments, resulting in reduced lifetimes and large maintenance expenses [1-3]. An example of this is the exposure of the oil industry transport infrastructure, usually made of steel AISI SAE 1020, to high temperatures and pressures when transporting crude oil and its derivatives [4]. Ceramic coatings act as an alternative method of corrosion and wear protection for these materials [4-6].

One thermal spraying technique using an oxyacetylene flame can be applied to protect and recover worn metal parts [4-7] by fabricating hundred-micron-thick coatings in one, two or more layers. For these coatings, an initial anchor layer (bond coat) is applied, which is usually a nickel-base alloy whose function is to improve the adhesion of the ceramic coating to the metal substrate and protect against corrosion [5-6]. For the wear and erosion protection of the metal substrate, it is common to use ceramic coatings of alumina (Al_2O_3), zirconia (ZrO_2) or titanium oxide (TiO_2), among others [6-7].

Alumina-zirconia coatings on steel AISI SAE 1020 have been prepared by atmospheric plasma spraying (APS) or high velocity oxy-fuel (HVOF), among other techniques [8,9], and they are expensive compared to thermal spray flame techniques. Therefore, in this work, bilayer coatings of ZrO_2-Al_2O_3/Ni were produced on substrates of steel AISI SAE 1020 using oxyacetylene flame thermal spraying with a spray distance of 8, 9 or 10cm, and two types of flames, oxidizing and super-oxidant. The objective was to evaluate the morphology, the wear and corrosion performances of these coatings.

MATERIALS AND METHODS

AISI SAE 1020 carbon steel substrates were used, and their surfaces were prepared by abrasive blasting with corundum particles (malla10-20) at a distance of 15 cm and an angle of 30º, The influence of the impact angle is still subject to controversy. However, all authors agree on the fact that if a surface is blasted at an angle between 45 and 90º Ra is not affected [4]. According to Pawlowski [10], using an angle of 30 degrees, an Ra of 5um is obtained, sufficient for the purposes of this investigation. Next, they were cleaned in an ultrasonic bath with ethyl alcohol to remove impurities, yielding an average roughness (Ra) of 4.9 ± 0.77 μm (an optimal result for coatings by oxyacetylene thermal spraying), which was measured using a profilometer Mitutoyo SJ 201 [4].

For fabrication of the coatings, commercial reference powders CPM 1205^{TM} and MetaCeram 25088^{TM} of commercial Castolin-Eutectic were used. The first was a base nickel-base alloy used for the bond coat, which counteracts the difference in thermal expansion coefficients of the substrate and the ceramic layer, improving adhesion. The second is a ceramic powder of ZrO_2-36 wt% Al_2O_3 used to exploit the good thermal properties of zirconia and the tribological properties of alumina. The chemical composition of the powders was obtained by X-ray fluorescence (XRF). The size distribution of the MetaCeram25088^{TM} particles was determined by laser dispersion (Master Size 2000E); meanwhile, the size distribution of the CPM 1205^{TM} was determined by analyzing the scanning electron microscopy (SEM) micrographs using Image-J software.

The coatings were deposited using an Areste I camera developed by the GIPIMME Group of the University of Antioquia (Colombia), which is equipped with a Castolin-Eutectic Terodyn 2000 torch and a RAYTEK infrared pyrometer to measure the surface temperature of the substrate, as well as the electromechanical systems that control the speed of the torch and the sample holder. The parameters used are presented for the both coating anchoring layer (CPM 1205^{TM}) and the ceramics powder (MetaCeram 25088^{TM}). In Table 1 a spray distance of 15cm was employed for the bond coat, along with an oxidizing flame obtained from a mixture of 59.46 L/min of O_2 with 21.18 L/min of C_2H_2. For the ceramic layer, three projection distances (8, 9 and 10cm) and two flames, an oxidizing flame obtained from a mixture of 59.46 L/min of O_2 with 21.18 L/min of C_2H_2 and a super-oxidant flame obtained from a mixture of 91.18 L/min of O_2 with 21.18 L/min of C_2H_2 were tested. The number of passes for the bond layer and the ceramic layer was 3 and 7, respectively. All of these parameters were obtained at the recommendation of the powder supplier and through pilot testing.

In Table 2, the sample designations are presented by the type of flame and the spray distance, where the letter O corresponds to an oxidizing flame, the letters SO correspond to a super-oxidant, and the numbers 8, 9 and 10 correspond to the torch-substrate distances in cm.

The porosity of the coatings was calculated from optical microscopy images of the cross-section of the samples according to the ASTM 2109-01 standard protocol [11].

The microhardness of the coatings was measured using a Vickers microhardness indenter (Shimadzu HMV-G). The critical load for the coatings obtained with the oxidizing flames and the super-oxidants was 120 and 150 g, respectively, with a hold time of 15 s. A total of 10 indentations were taken in air at room temperature in accordance with the ASTM 1327-08[12] standard protocol.

The surface morphology and cross section of the samples were evaluated using SEM at a high magnification. The samples were prepared according

Table 1. The thermal spraying parameters of the coatings MetaCeram 25088^{TM} and CPM 1205^{TM}.

Parameter	MetaCeram 25088^{TM} [ZrO_2-Al_2O_3]			CPM 1205^{TM}
Pressure O_2 (Psi)	50			50
Pressure C_2H_2 (Psi)	12			12
Pressure N_2 (Psi)	40			40
Pressure air (Psi)	30			30
Flow O_2 (l/min)	59.46*		91.18*	59.46*
Flow C_2H_2 (l/min)	21.18*		21.18**	21.18*
Flow N_2 (l/min)	17			17
Speed torch (cm/s)	0.59			0.72
Speed sample holder (rpm)	116			116
Preheating temperature (ºC)	155	160	196	233
Substrate emissivity	0.685			0.8
Passes projection	7			3
Projection distance (cm)	8	9	10	15
Powder flow (g/min)	9			46.8

* Oxidizing flame. ** Super-oxidant flame.

Table 2. The sample designations according to the type of flame and spray distance.

Designation	Flame type	Projection distance (cm)
O_8	Oxidizing	8
O_9		9
O_{10}		10
SO_8	Super-oxidant	8
SO_9		9
SO_{10}		10

to ASTM E 1920-03 [13]. MicroTest tribometer was used in the ball-disk configuration to test the wear. A sphere of polished alumina 6 mm in diameter was used as the ball, and disc-shaped coated substrates 2.56 cm in diameter and 1cm thick were used. They were polished with abrasive SiC paper until an average roughness (Ra) of 11.12 ± 0.24 µm was obtained. After, they were subjected to wear tests while the following parameters were held constant: a disk speed of 95.5 rpm for 20000 cycles, a load of 5 N and a sliding speed of 0.1 m/s; the diameter of the track was 10 mm with a distance of 1256.6 min 3.5 hours. The wear rate (W.R) was calculated using equation (1), as reported by [6,14].

$$\text{W.R.} = \frac{\textit{Wear volume}}{\textit{Load} \times \textit{distance covered}} = \frac{2\pi r A_d}{P 2\pi r N_c} = \frac{A_d}{P N_c} \quad (1)$$

Where Ad is the area of the profile of the mark on [µm^2]. A_d was determined from 10 measurements of the wear track, for which a Leica-brand confocal microscope was used.

The corrosion resistance was evaluated by electrochemical impedance spectroscopy (EIS) using a Gamry galvanostat potentiostat. The polarization experiments were performed using an electrochemical cell with three electrodes. Steel was used as the working electrode, a platinum wire as the counter electrode and a silver chloride electrode as the reference electrode. An electrolyte solution of 0.012% acetic acid with a pH of 5.5 was also used. Acetic acid is commonly used as an electrolyte buffer to evaluate corrosion in low-density coating systems or thin films using electrochemical methods. The pH values can be maintained at 6 to avoid excessive production of H2, thus controlling the damage against the iron substrate and allowing evaluation of the coating performance as a function of the spray parameters. Also, acetic acid allows adding controlled ion concentrations such as Cl- and Br- without modifying the pH level, to evaluate the coating damage of these ions [15-18].

Electrochemical impedance tests (EIS) were performed at a potential frequency of Vrms = 5 mV amplitude in an open circuit potential. Electrochemical impedance tests (EIS) were performed at a frequency of 10^5-10^{-1} Hz, with a potential amplitude of Vrms = 5mV.

RESULTS AND DISCUSSION

Chemical composition and morphology of the starting powders (MetaCeram 25088™ and CPM1205™)

In Table 3, the XRF results of the chemical composition of the powders and CPM1205™ MetaCeram 25088™ are shown. It is noted that the powders used as the bond coats have a 97.62 wt% of Ni, 1.79 wt% Si and small amounts of iron, aluminum and copper.

Table 3. Chemical composition of the powders XRF MetaCeram 25088™ and CPM 1205™.

MetaCeram 25088 ™		CPM 1205™	
Compound	**(wt%)**	**Element**	**(wt%)**
ZrO_2	59.72	Ni	97.62
Al_2O_3	35.7	Si	1.79
HfO_2	0.94	Fe	0.34
MgO	0.35	Al	0.18
Y_2O_3	0.25	Cu	0.07
Others	2.74		

The particle size distribution obtained for the MetaCeram 25088™ ranged between 15 and 94 µm with an average size of 50 µm; meanwhile, the powder CPM 1205™ ranged between 20 and 70 µm, with an average size of 31 µm.

The analysis of the morphology of the powders was performed using SEM micrographs. In Figure 1, the powder morphology of MetaCeram 25088™ is observed (see Fig. 1a); it consisted of spherical particles of micrometer agglomerated and sintered alumina nanoparticles (dark areas) and zirconia (light areas) [19], (see the cross-section of a microsphere, Fig. 1a').

For the material of bond coat (CPM 1205™), the micrometric particles are round or oval, and they are obtained by spraying (spray dry) in water (see Fig. 1b) [10]. A cross section of these particles (see Fig. 1 b ') illustrates that some are hollow, which facilitates their melting in the flame.

ANALYSIS OF THE MORPHOLOGY OF COATINGS

Bond coat (CPM 1205™)

In Figure 2, the morphology is presented in the SEM images of the nickel-base alloy (CPM

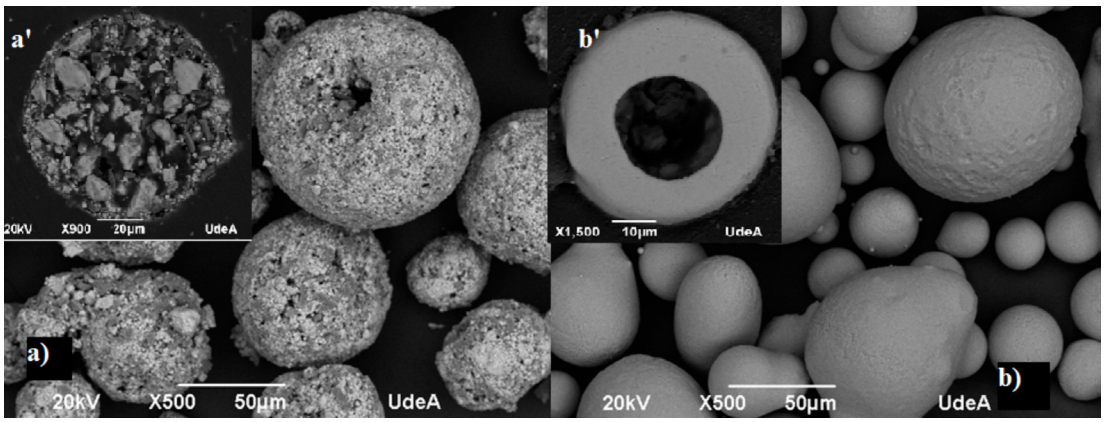

Figure 1. Micrograph powders. a) MetaCeram 25088^{TM}. b) CPM powder 1205^{TM}.

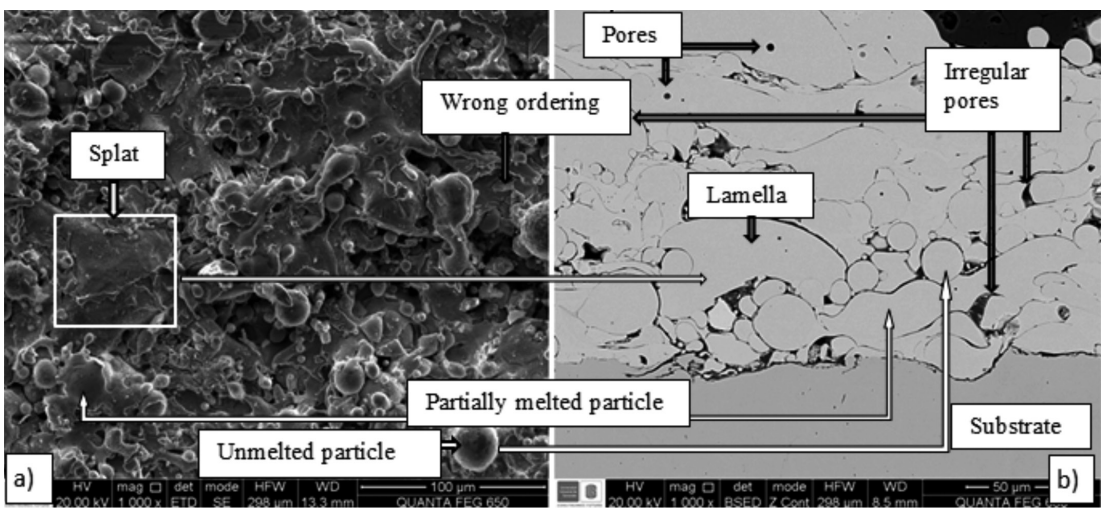

Figure 2. The morphology of the bond coat (CPM 1205^{TM}) by SEM: (a) the surface view and b) the cross-sectional view.

1205^{TM}) coating used as a bond coat. Lamellae were observed having formed from the completely melted particles of different sizes, and the stacking faults and macrospores of such coatings are also noted. An average thickness of 249 microns was measured, with an average porosity of 4.9 ± 1.6%, which is lower than the thicknesses reported by other authors (7.2 ± 1.6% and 23.7 ± 3.4%) for similar coatings [20,21]. The parameters used for the projection of this layer (see Table 1) are therefore considered suitable because they allow the largest amount of particles of the starting powder to melt, which then optimally adhere to the substrate with a lower porosity.

Layer of ZrO_2-36%Al_2O_3 (MetaCeram 25088^{TM})

In Figures 3 to 8, the morphology of the coatings of ceramic layer (MetaCeram 25088^{TM}) samples O8, O9, O10 are presented (for SO8, SO9, SO10, see Table 2). Part a) of Figures 3 to 8 corresponds to the coating surfaces, where the following main features are observed: splats (1), bimodal areas (2), cracks (3), pores produced by particle evaporation (4) and (5). Meanwhile, part b) corresponds to the micrograph of a cross section of the coating in which the following features are observed: lamellae (1), bimodal areas (2), cracks (3), pores (4), stacking faults (5) and the substrate (6). The

splashes are formed when the melted particles are hitting the surface are flattened to form a disc or splash shape. The lamellae are the result of molten particles and form parallel to the substrate. Bimodal areas result from agglomerated nanoparticles (see Figure 1a), which, at the time of passing through the flame, are partially melted leaving unmelted particles trapped by others that have completely melted. The formation of these areas was also reported for these same coatings by A. González et al. [22], although in smaller quantities, but they used atmospheric plasma spraying. This type of bimodal area improves the mechanical properties of the coatings, such as the prevention of fracture resistance and crack propagation by dissipating energy in the nanometric areas [14, 19].

The cracks are generated by the impact and rapid solidification of the splat and are typical of this type of coating [6, 7, 10, 23, 24]. Stacking defects occur from the irregularities of the substrate or a previously deposited layer [14]. The circular pores correspond from the partial evaporation of particles.

In the images (Figures 4 to 9), areas of white, dark gray and light gray appear; the white areas correspond to the ZrO_2 phase. Dark gray corresponds to the Al_2O_3 phase, and light gray lamellae are associated with a solid solution of ZrO_2 and Al_2O_3 and correspond to these phases: $m - ZrO_8$ $Al_{12}O_{8(corindon)}$, $t - Zr_2O_{3.94}$, $c - Zr_4O_8$. In Figure 3, you can see the present phases as two amorphous zones, the first between 24 and 36 degrees and the second between 53 and 65 degrees. Some investigators reported similar

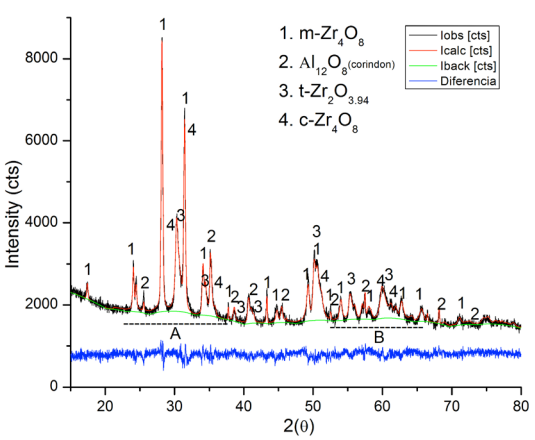

Figure 3. XRD pattern O8 coating obtained with an oxidizing flame at a distance of 8cm.

results in coatings made with the same powder using atmospheric plasma spraying (APS) and plasma but with the raw material in a suspension [19, 25].

Porosities of approximately 5% for the coatings obtained with an oxidizing flame and between 6 and 9% for the super-oxidizing flame were found (see Table 4). This demonstrates the relationship between the porosity and the type of flame, where the porosities of the coatings obtained with oxidizing flames are lower than those obtained with super-oxidizing flames; this sort of behavior was also found by C. Cano *et al.*, who noticed that, by lowering the flame temperature, the splat size decreases and the amount of unmelted particles increases, therefore, increasing the porosity [26].

The results show that the porosity tends to decrease as the projection distance increases. As the projection distance increases, the number of particles that are deflected is lower because the kinetic energy decreases, resulting in a more uniform coating.

The porosity of the coatings obtained with the same powder and the same technique, but with the thermal spray parameters, is lower in this work than the porosities reported by A. Gonzalez *et al.* They report porosities between approximately 15% and 18% [20].

MICROHARDNESS AND WEAR OF CERAMIC COATINGS (METACERAM 25088^{TM}).

In Table 4, the percentage of porosity, Vickers microhardness and wear rate of the ceramic coatings are reported. It is noted that there is no relation between the microhardness and the type of flame and spray distance (8, 9 and 10cm) with very similar results ranging from 7.8 ± 0.6 and 8.6 ± 0.4 GPa. It is known that measuring the microhardness of coatings obtained by thermal spraying is widely affected by the defects [7,10]. For each hardness measurement, at least 20 indentations were performed, but only 10 filled the requirements of the standard protocol [12]; the selected traces were normally in well melted areas of the coating well, and this is why the microhardness values are similar for all samples. When comparing the values obtained in this work with those reported by other authors, the coatings obtained by flame spraying were found

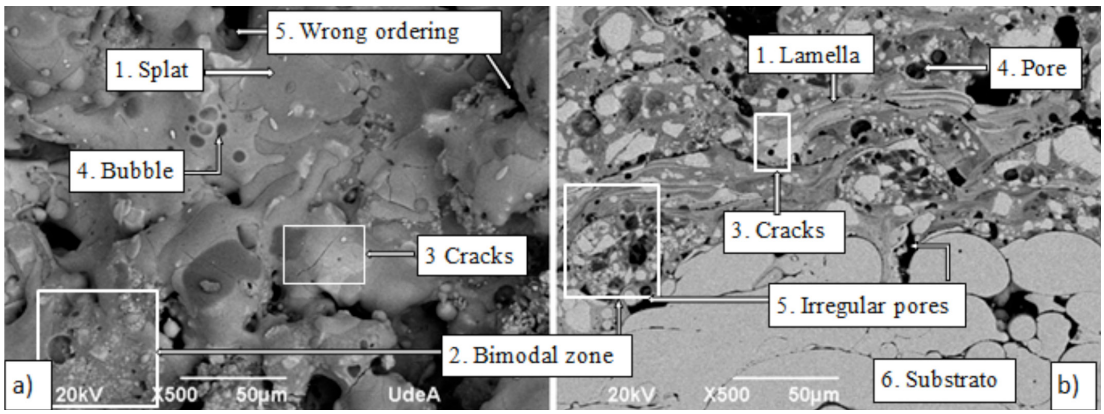

Figure 4. The morphology of the O8 sample: a) the surface and b) the cross- section of the coating.

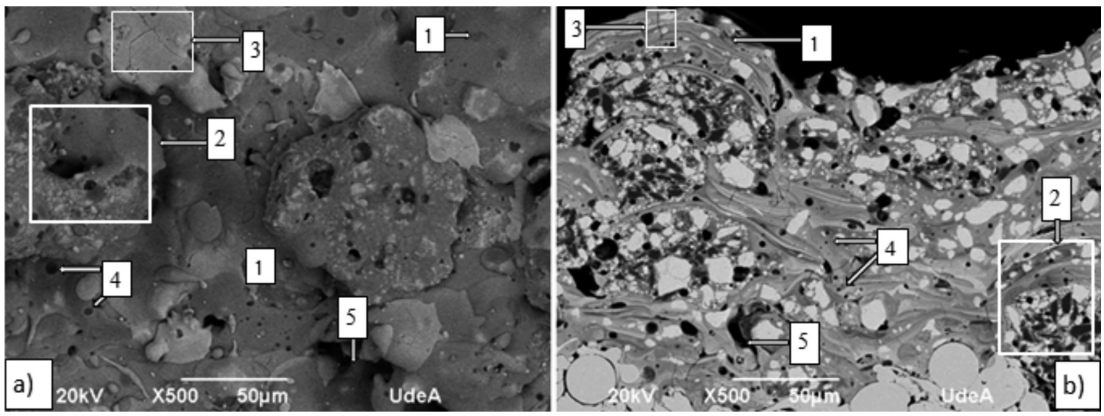

Figure 5. The morphology of the O10 sample: a) the surface and b) the cross- section of the coating.

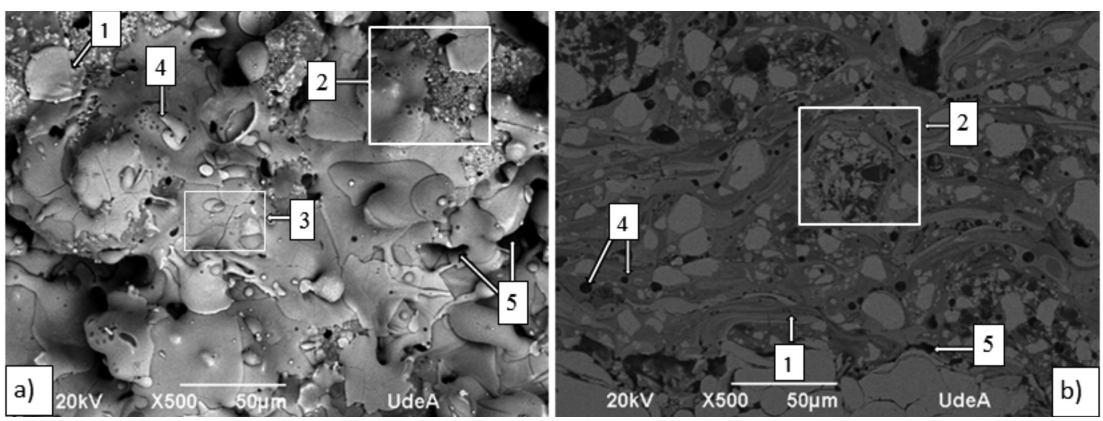

Figure 6. The morphology of the O10 sample: a) the surface and b) the cross- section of the coating.

to have microhardnesses ranging between 2.02 and 6.22 GPa [20], while the coatings obtained using the same powder but with the APS technique have microhardnesses of 10.1 GPa [22], which is greater than the one found in this work. The larger value is justified by a lower percentage of porosity and

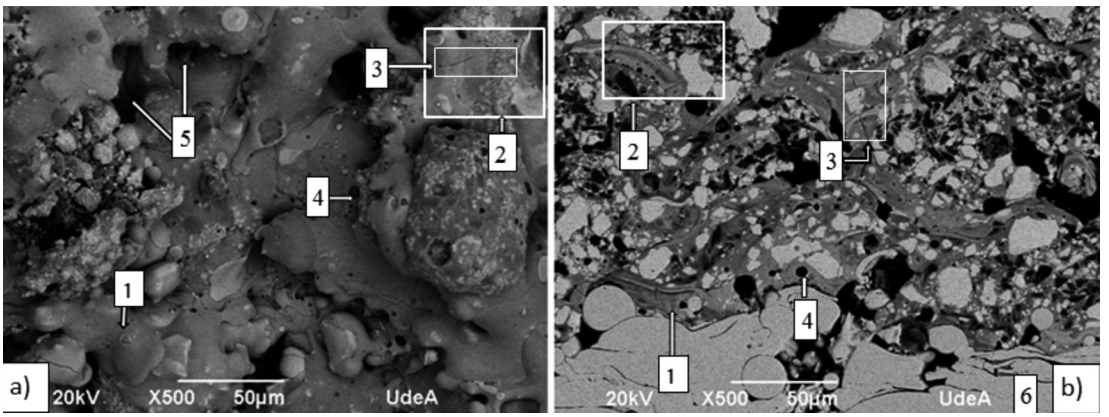

Figure 7. The morphology of the O10 sample: a) the surface and b) the cross- section of the coating.

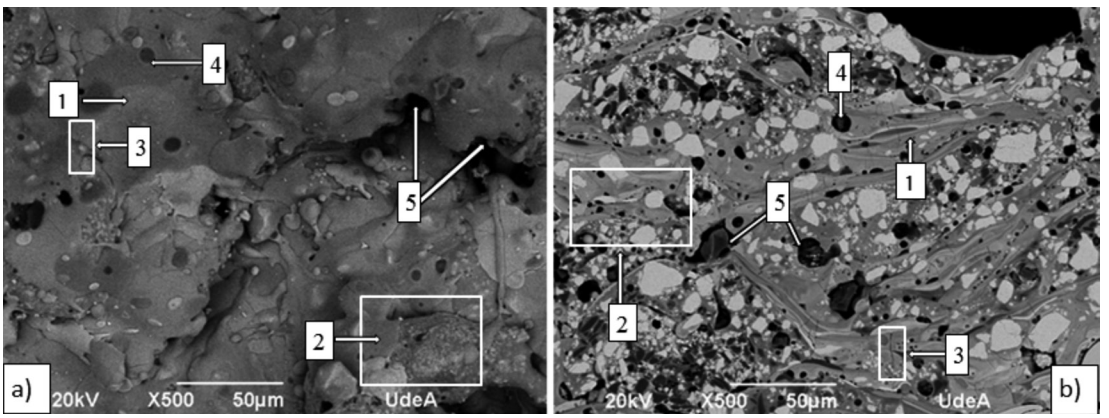

Figure 8. The morphology of the SO10 sample: a) the surface and b) the cross- section of the coating.

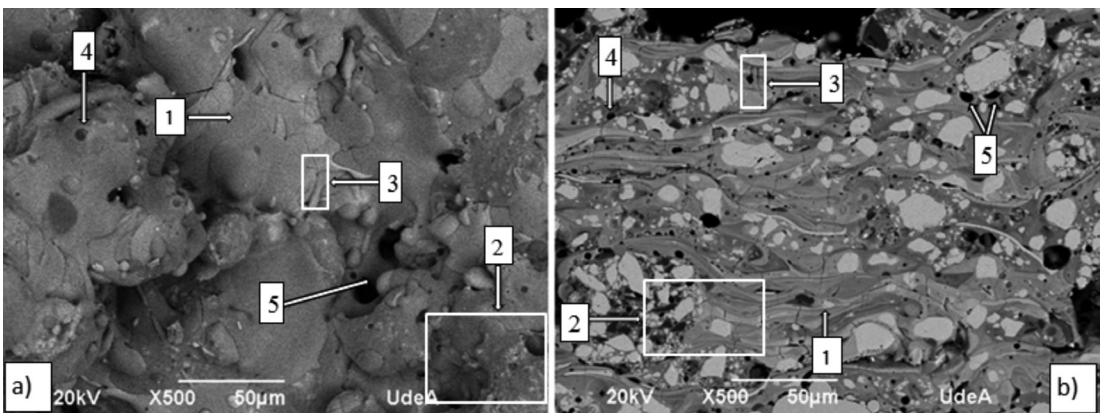

Figure 9. The morphology of the SO10 sample: a) the surface and b) the cross- section of the coating.

a greater amount of molten particles, which was expected for coatings obtained by APS.

From the results of wear resistance, it is observed that all are of the same order of magnitude, ranging between 1.2×10^{-4} and 2×10^{-4} mm^3/Nm. These, are higher than those reported by A. González *et al.* (4.6×10^{-5} mm^3/Nm) [22] and J. Suffner *et al.* ($11.03\pm0.17\times10^{-5}$ mm^3/Nm) [19], who used APS to obtain the coatings. In Figure 10, the morphology

of the wear surface is shown for the test on S08 sample. The images of the other samples are similar, and for this reason, they are not presented here. The observed ductile deformation zones were caused by the contact between the coating and the alumina ball used as the counterbody [27]. This phenomenon generates withdrawn particles (debris) and abrasion marks on the surface (grooves). The particles are broken away or detached (debris) also generate plastic deformation, and the hardest ones tilled the softer surface to produce edges that were flattened with the contact of the passing ball, and they formed continuous protrusions that become flakes during the plastic deformation wear [27].

ELECTROCHEMICAL CORROSION TESTS

In Figure 11, the Bode plot for a sample of bare steel is presented, and Figures 12 and 13 show the diagrams for samples coated using an increasing oxidizing and super-oxidant flame, respectively. From these it is seen that low frequency steel has a polarization resistance (Rp) of 4.908 KOhm, which is similarly reported in reference [28] for the same type of steel.

It is clear that for the coatings made with a super-oxidizing flame, the resistance during polarization is greatly increased as the spray distance increases (see Figure 13), indicating an improvement in the ability of protecting against corrosion. This was also observed in the morphology of the coatings, where, at a greater spray distance, the surface morphology was more uniform (see Figures 7, 8, 9) resulting in a lower porosity (see Table 4). Furthermore, it was inferred that, for coatings made with an oxidizing flame, shorter distance projection resulted in a higher polarization resistance (see Figure 12).

Also in Figures 12 and 13, the effects of the two types of metal (Ni and Steel) are observed because two elements of constant phase are observed: the first is between 100 and 1 kHz, and the second is between 1 and 0 Hz. This indicates that nickel forms its own element of constant phase. Table 5 lists the polarization resistance for each of the samples.

According to the results reported in Table 5, coating a bilayer of coatings of ZrO_2-Al_2O_3/Ni protects the substrate in the worst case, approximately 27 times better than if it were uncoated. Therefore, the coatings can be used to protect steel surfaces (AISI SAE 1020) exposed to corrosive environments.

Table 4. The mechanical properties of the coatings (MetaCeram 25088TM).

Sample	Porosity [%]	Average pore area [μm^2]	Microhardness Vickers [GPa]	Wear rate $\times10^{-4}$ [mm^3/N.m]
O8	5.3 ± 0.9	14.9 ± 1.2	7.8 ± 0.6	1.3 ± 0.07
O9	5.1 ± 0.9	15.4 ± 1.7	8.4 ± 0.9	2.1 ± 0.20
O10	5.4 ± 1.2	16.1 ± 1.6	8.6 ± 0.3	2.1 ± 0.46
SO8	9.1 ± 1.1	18.2 ± 1.3	8.0 ± 0.4	1.2 ± 0.13
SO9	6.9 ± 1.1	17.7 ± 1.5	8.3 ± 0.4	1.7 ± 0.31
SO10	5.8 ± 0.9	17.0 ± 1.9	8.2 ± 0.6	1.3 ± 0.20

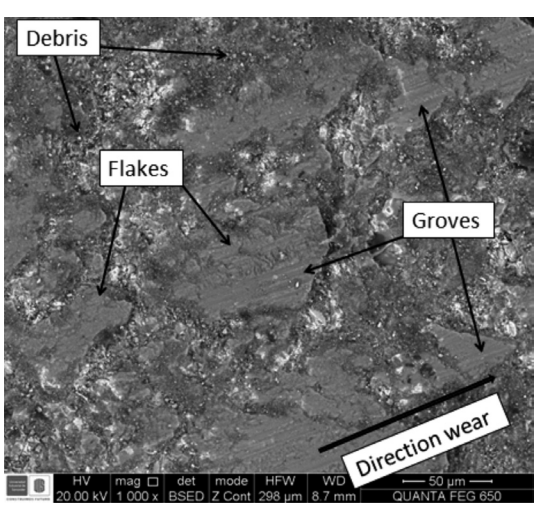

Figure 10. The morphology of the wear track of the SO8 coating.

Table 5. The polarization resistance of the bilayer coatings ZrO_2-Al_2O_3/Ni for different configurations.

Sample	Polarization resistance (KOhm)
O8	224.4
O9	194.6
O10	188.7
SO8	130.9
SO9	175.4
SO10	233.4
AISI SAE 1020	4.908

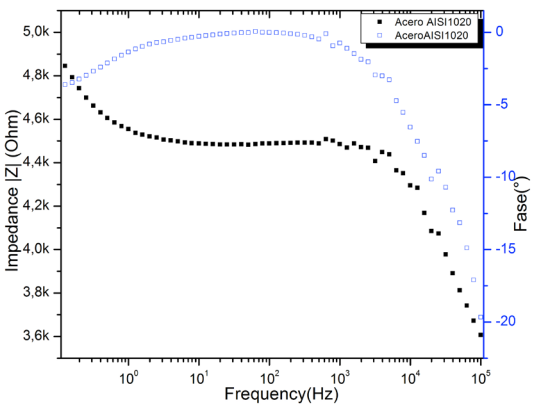

Figure 11. The Bode diagram for steel AISI SAE 1020 in a solution of 0.012% acetic acid with a pH of 5.5.

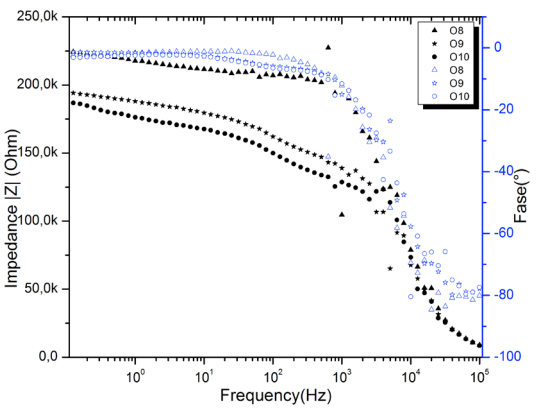

Figure 12. The Bode diagrams for O8, O9 and O10 samples in a solution of 0.012% acetic acid with a pH of 5.5.

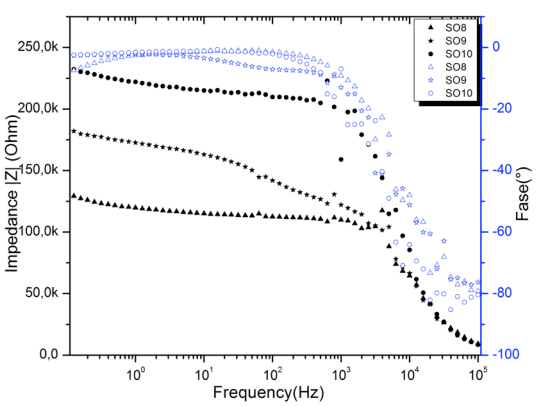

Figure 13. The Bode diagrams for coated SO8, SO10, SO9 and substrates in a solution of 0.012% acetic acid with a pH of 5.5.

CONCLUSIONS

Bilayer coatings (ZrO_2-Al_2O_3/Ni) were elaborated by oxyacetylene thermal spraying on steel substrates AISI SAE 1020. The first layer (bond coat) was fabricated using a commercial powder of a nickel-base alloy (CPM1205™) with an oxidizing flame and a spray distance of 15 cm. The second layer is made from a mixture of ZrO_2-36 wt% Al_2O_3 (MetaCeram 25088™) applied using both super oxidant and oxidant flames at spray distances of 8, 9 and 10 cm.

The morphology of the bond layer (CPM1205™) demonstrates the formation of lamellae from completely molten particles, and the stacking faults and micropores of these coatings are also acknowledged.

For the ceramic layer, the morphology of the surface and the cross section of the coating were evaluated, showing the formation of bimodal areas due to nanoparticulate agglomerations in other micrometric agglomerations that, when crossing the flame, are partially melted, leaving unmelted particles trapped by melted particles.

The results of Vickers microhardness and wear resistance tests for the ceramic coatings do not change when varying the type of flame and the spray distance (8, 9 and 10 cm).

It was evident that using a super oxidant flame, the resistance to polarization increases as the spray distance increases; meanwhile, for samples with the oxidizing flame, the opposite behavior was observed. When comparing the corrosion resistance of the steel substrate AISI SAE 1020 and the coated samples, a significant increase was observed, meaning that these bilayer coatings can be used to protect steel surfaces AISI SAE 1020 exposed to corrosive and erosive environments, thus demonstrating the utility and versatility of the flame spray technique.

ACKNOWLEDGMENTS

A Sustainability Strategy 2014-2015 at the Universidad de Antioquia allowed GIPIMME group participation in the development of the coatings.

REFERENCES

[1] D. Toma, W. Brandl, G. Marginean. "Wear and corrosion behaviour of thermally sprayed cermet coatings". Surf. Coatings Technol. Vol. 138, pp. 149-158. 2001

[2] A. Al-Odwani, M. Al-Tabtabaei, A. Al-Hashim, J. Carew, F. Al-Atram. "Erosion of construction materials in a reverse osmosis plant utilizing seawater in Kuwait". Desalination.Vol. 129, pp. 137-145. 2000.

[3] M.M. El Rayes, H.S. Abdo, K.A. Khalil. "Erosion-Corrosion of Cermet Coating". Int.J.Electrochem.Sci. Vol. 8, pp. 1117-1137. 2013.

[4] J.R. Davis. "Handbook of Thermal Spray Technology". ASM International, 2004.

[5] Y. Arata, A. Ohmori, Ch-J.Li. "Electrochemical method to evaluate the connected porosity in ceramic coatings". Thin Solid Films. Vol. 156, pp. 315-326. 1988.

[6] F. Vargas, H. Ageorges, P. Fauchais, M.E. López, J.A. Calderon. "Permeation of saline solution in Al2O3-13wt.% TiO2 coatings elaborated by atmospheric plasma spraying". Surf. Coatings Technol. Vol. 220, pp. 85-89. 2013.

[7] P. Fauchais, J. Heberlein, M. Boulos. "Thermal Spray Fundamentals From Powder to Part". Springer. First Edition. New York, USA. pp. 1566. 2014. ISBN 978-0-387-28319-7.

[8] F. Vargas. "Élaboration de couches céramiques épaisses à structures micrométriques et nanométriques par projections thermiques pour des applications tribologiques". Limoges, 2010. http://epublications.unilim.fr/theses/2010/vargas-fabio/vargas-fabio.pdf.

[9] Y. Wang, C.G. Li, W. Tian, Y. Yang. "Laser surface remelting of plasma sprayed nanostructured Al2O3-13wt%TiO2 coatings on titanium alloy". Appl. Surf. Sci. Vol. 255, pp. 8603-8610. 2009.

[10] L. Pawlowski. "The Science and Engineering of Thermal Spray Coatings". John Wiley & Sons. Second Edition. Chichenster, England. pp. 626. 2008. ISBN 978-0-471-49049-4.

[11] ASTM E2109-01. "Standard Test Methods for Determining Area Percentage Porosity in Thermal Sprayed Coatings".

[12] ASTM C1327-08. "Standard Test Method for Vickers Indentation Hardness of Advanced Ceramics 1".

[13] ASTME1920-03."Standard Guide for Metallographic Preparation of Thermal Sprayed Coatings 1".

[14] A.G. González. "Estudio del comportamiento a alta temperatura de recubrimientos nanoestructurados elaborados por proyección térmica por combustión y plasma a partir de polvos y suspensiones" Tesis doctoral. 2014.

[15] F. Stippich, E. Vera, H. Scheerer, G.K. Wolf, X. Jian-Ming. "Corrosion properties of alumina coatings on steel and aluminum deposited by ion beam assisted deposition". Surf. Coatings Technol. Vol. 98, pp. 997-1001. 1998.

[16] E. Vera, G. Wolf. "Optimisation of TiN-IBAD coatings for wear reduction and corrosion protection, Nucl". Instruments Methods Phys. Res. Sect. B Beam Interact. with Mater. Atoms. Vol. 148 pp. 917-924. 1999.

[17] V. Pavlík. "Corrosion of hardened cement paste by acetic and nitric acids part I: Calculation of corrosion depth". Cem. Concr. Res. Vol. 24, pp. 551-562. 1994.

[18] A. Turnbull, M. Ryan, A. Willetts, S. Zhou. "Corrosion and electrochemical behaviour of 316L stainless steel in acetic acid solutions". Corros. Sci. Vol. 45, pp. 1051-1072. 2003.

[19] J. Suffner, H. Sieger, H. Hahn, S. Dosta, I.G. Cano, J.M. Guilemany. "Microstructure and mechanical properties of near-eutectic ZrO2-60 wt.% Al2O3 produced by quenched plasma spraying". Mater. Sci. Eng. A. Vol. 506, pp. 180-186. 2009.

[20] A. Gonzalez, J. Henao, A.F. Diaz, E. López, F. Vargas. "Influencia de los parámetros de proyección térmica en la microestructura de los recubrimientos de circona-alúmina y circona-ceria usados como barreras térmicas" Rev. Latinoam. Metal. y Mater. Vol. 33, pp. 272-281. 2013.

[21] J.E. Montoya, F. Vargas, J.A. Calderón. " Evaluación de la Capacidad Protectora de Recubrimientos Ni-SiC y Ni-Co-W Depositados por Proyección Térmica". Dyna. Vol. 76, Núm. 160, pp. 200, 202. 2009.

[22] A.G. González, H. Ageorges, O. Rojas, E. López, F.M. Hurtado, F. Vargas. "Efecto de la microestructura y de la microdureza sobre la resistencia al desgaste de recubrimientos elaborados por proyección térmica por plasma atmosférico a partir de circona-alúmina,

circona-itria y circona-ceria". Boletín La Soc. Española Cerámica Y Vidr. Vol. 54, Issue 3, pp. 124-132. May-June 2015.

[23] M. Rezvani, G.H. Farrahi, M. Azadi, M. Ghodrati. "Effects of preheating temperature and cooling rate on two-step residual stress in thermal barrier coatings considering real roughness and porosity effect". Ceram. Int. Vol. 40, pp. 15925-15940. 2014.

[24] M. Nejati, M.R. Rahimipour, I. Mobasherpour, A.H. Pakseresht. "Microstructural analysis and thermal shock behavior of plasma sprayed ceria-stabilized zirconia thermal barrier coatings with micro and nano Al2O3 as a third layer". Surf. Coatings Technol. Vol. 282. pp. 129-138. 2015.

[25] A. González, E. López, A. Tamayo, E. Restrepo, F. Hernández, "Análisis de la microestructura y de las fases de elaborados por proyección térmica". Dyna. Año 77, Nº 162, pp. 151160. Medellín, Junio. 2010. ISSN 00127353.

[26] C. Cano, M.I. Osendi, M. Belmonte, P. Miranzo, "Effect of the type of flame on the microstructure of CaZrO3 combustion flame sprayed coatings". Surf. Coatings Technol. Vol. 201, pp. 3307-3313.

[27] D.H. Mesa Grajales. "Principios de Tribología" Universidad Tecnológica de Pereira Colombia. pp. 305. 2007. ISBN 9588272254, 9789588272252.

[28] G. Capote, G. Mastrapa, J.J. Olaya. "Resistencia al desgaste y a la corrosion de recubrimientos de dlc depositados sobre aceros AISI 304 y AISI 1020" . Rev. Latinoam. Metal y Mater. Vol. 35, pp. 134-141.